Journal of Thermal Analysis and Calorimetry, Vol. 72 (2003) 777–789

KINETICS OF THE OXIDATION OF MAGNETITE USING SIMULTANEOUS TG/DSC

J. P. Sanders [1] *and P. K. Gallagher* [2]

[1]National Brick Research Center, 100 Clemson Research Park, Anderson, SC 29625, USA
Adjunct Prof., Department of Ceramic & Materials Eng.
[2]Emeritus Prof., Departments of Chemistry and MS&E, The Ohio State University, Columbus, OH 43210, USA; Adjunct Prof., Departments of Chemistry and Ceramic & Materials Eng., Clemson University Clemson, SC 29632, USA

Abstract

Kinetics of the oxidation of magnetite (Fe_3O_4) to hematite (α-Fe_2O_3) are studied in air using simultaneous TG/DSC. The mechanism is complex and the differences between the kinetic conclusions and Arrhenius parameters based on either TG or DSC are discussed. As in our previous work on $CaCO_3$ [1], the determination of a satisfactory baseline for the DSC results adds considerable uncertainty to those kinetic results. Consequently the calculations based on the TG data are considered superior.

Solid state reactivity varies from one source of material to another and the results are compared for two different commercial samples of magnetite, both presumably prepared by wet chemical methods. These materials are much more reactive than the material studied previously [2], which had been coarsened and refined at high temperatures. In that earlier study, the metastable spinel, γ-Fe_2O_3, was formed as an intermediate in the oxidation to the final stable form, α-Fe_2O_3.

The exothermic reaction of the gamma to alpha form of the product during the oxidation process destroys the direct comparison between the TG and DSC results, since the former only detects the change in mass of the sample and not the crystallographic transformation. The TG results, however, represent the true oxidation process without superposition of the structural aspects.

Keywords: kinetics, oxidation of magnetite, simultaneous TG/DSC

Introduction

Magnetite, Fe_3O_4, is metastable in air below about 1000ºC compared to the fully oxidized hematite, α-Fe_2O_3 [3]. Consequently, the existence of magnetite at lower temperatures is dependent on its kinetic stability. The reactivity of magnetite therefore depends on many factors, e.g., surface area, impurities, defects, etc. Previous work [2] on high temperature annealed, coarse powder indicated oxidation only above 500ºC. Magnetite prepared at relatively low temperatures from freshly precipitated precursors, however, has a much greater surface area and defect concentration and therefore oxidizes at much lower temperatures [4]. Regardless of the temperature at which the magnetite is oxidized, the process has been shown to go through the intermediate product, metastable γ-Fe_2O_3 [2, 4].

1388–6150/2003/ $ 20.00
Akadémiai Kiadó, Budapest

The exothermic metastable to stable transition should accompany the exothermic oxidation process and be reflected in the DTA or DSC curve. Only the oxidation process involves a change in mass and thus the TG curve will ignore the crystallographic transformation, except for any self-heating effects. This creates an interesting test for comparison of the kinetics for this overall oxidation process as derived from TG with that determined based on DSC or DTA. Such a comparison has been made for the endothermic decomposition of $CaCO_3$ [1]. In that case, however, the presence of an intermediate amorphous phase could only be speculated. In addition, that decomposition is readily reversible and thus subject to greater uncertainties. The oxidation of magnetite offers a better test case for the comparison of kinetics derived separately from simultaneous TG and DTA or DSC measurements.

Experimental procedures

The sources of magnetite were Aldrich high purity grade (material A) and Alpha, Puritonic grade (material B). A series of experiments was performed using 10.6±0.5 mg sample sizes. The atmosphere was flowing 20% O_2 in N_2 at a rate of 1.0 L min^{-1}.

Simultaneous TG/DSC was performed using a Netzsch Model 449C instrument with its SiC furnace. Samples were contained in the manufacturer's alumina crucibles. The Puratronic material was used as is since it was a uniformly fine chemically precipitated material. The Aldrich material consisted of a wide range of particle sizes and was therefore screened to –200 mesh (74 micron) prior to analysis. Both TG and DSC baselines were corrected by subtraction of predetermined baselines run under identical conditions except for the absence of sample. Five nominal heating rates, 1, 2, 4, 8 and 16ºC min^{-1}, were performed and the materials were typically heated to 800°C to ensure complete oxidation. A 5 mg sample of high purity (99.997%) In foil from AESAR was run at 8ºC min^{-1} in dry Ar to determine the correction constants used in the subsequent kinetic analysis.

The Netzsch Proteus and Thermokinetics software packages [5] were used for data analysis. In the least squares fitting during the kinetic analysis of the TG data no weighting factors were applied to the data. For the DSC measurements tangential baselines and weighting factors of $1/(Y_{max}^2 + Y_{min}^2)$ were applied to the data. Instrumental correction factors (temperature dependence=0.00063, thermal resistance=0.1464 K mW^{-1}, filter=2 low pass, τ_1=0.1201 s, τ_2=0.1049 s, τ_3=25.6150 s), determined by the software using the curve for the melting of Al, were factored into the DSC kinetic analysis. These correction factors are used where the measurement itself causes some distortion of the signal. These correction factors are for desmearing functions and thermal resistance corrections. Sources of this distortion relate to thermal transport properties of the materials used for the crucible and measuring head and the latter's configuration.

Results

The screened Aldrich material had a mass gain closer to the theoretical value of 3.46 mass%. The curves for the Puritonic material were similar qualitatively but less consistent in their behavior as a function of heating rate. This suggested some inhomogeneity and only the data for material A are reported herein.

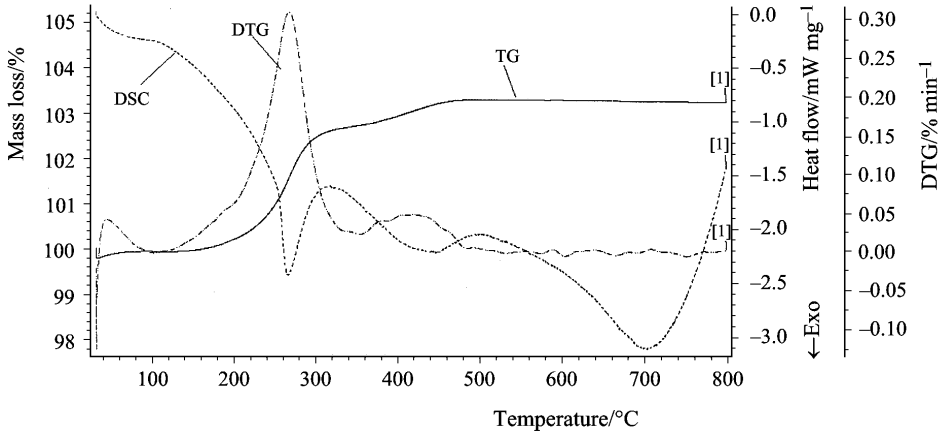

Fig. 1 Simultaneous TG/DSC curves for the oxidation of magnetite at 8°C min^{-1} in 20% O_2, 80% N_2

Figure 1 shows a representative result for the simultaneous TG/DSC at an intermediate heating rate, 8ºC min^{-1}. The full data sets which serve as inputs to the kinetics software are shown in Figs 2 and 3. Table 1 presents selected data from these curves. The separation between the two peaks at each heating rate is based on the point of inflection in the TG curve. No peak resolution or deconvolution analyses were performed to obtain the areas associated with each peak.

Table 1 Selected values for the simultaneous TG/DSC of magnetite

Heating rate/ °C min^{-1}	Sample mass/mg	DTG peak/°C	Mass gain/ mass%	DSC peak/°C
1	10.1	235.6	2.75	235.1
1		Undetermined	0.78	351.9
2	10.7	244.8	2.72	240.0
2		365.1	0.81	367.9
4	11.1	255.5	2.75	252.5
4		404.2	0.72	397.3
8	10.3	268.7	2.78	266.6
8		422.4	0.61	439.6
16	10.3	281.1	2.77	281.3
16		425.4	0.66	438.4

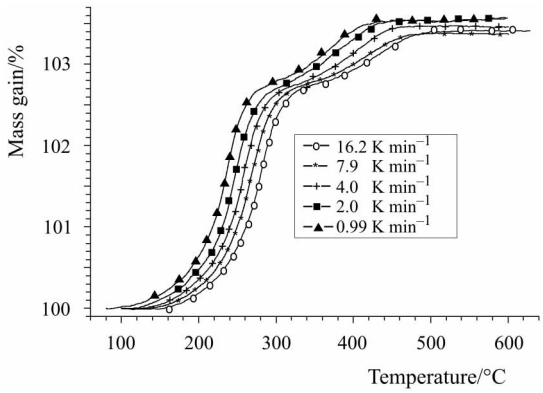

Fig. 2 TG curves for the oxidation of magnetite in 20% O_2, 80% N_2

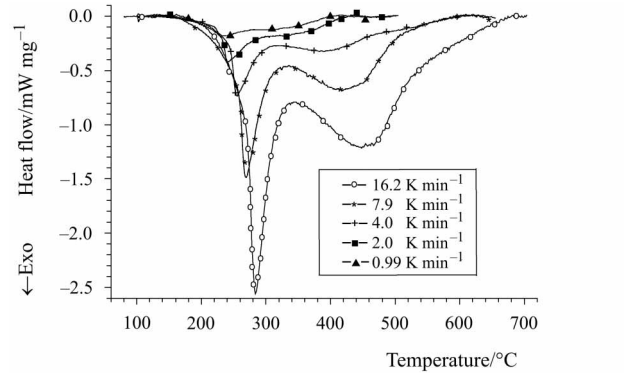

Fig. 3 DSC curves for the oxidation of magnetite in 20% O_2, 80% N_2

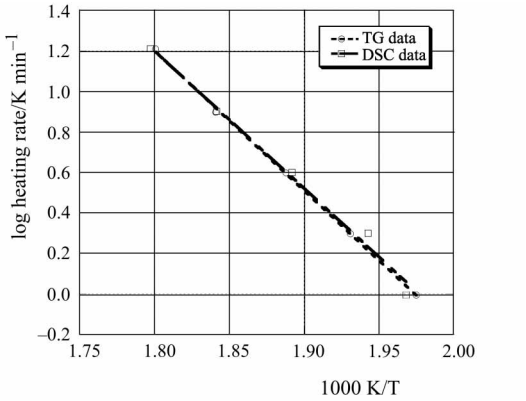

Fig. 4 ASTM plot of the kinetic analysis for the oxidation of magnetite

All three types of model-free kinetic analyses available in the thermokinetics software were used on both data sets shown in Figs 2 and 3. Results from the ASTM based analysis are presented in Fig. 4 and Table 2. Table 3 and Fig. 5 summarize the kinetic pa-

rameters derived from the Friedman approach. Outcome from the Flynn–Ozawa analysis is given in Table 4 and Fig. 6.

Table 2 Selected results from the ASTM model-free kinetic analyses

Technique	E_a/kJ mol^{-1}	log$A$/s^{-1}
TG	124±2	9.68
DSC	121±7	8.85

Table 3 Selected results from the Friedman model-free kinetic analyses

Technique	E_a/kJ mol^{-1}	log$A$/s^{-1}
TG	230–65	24–4.0
DSC	128–23	8.4–(–0.8)

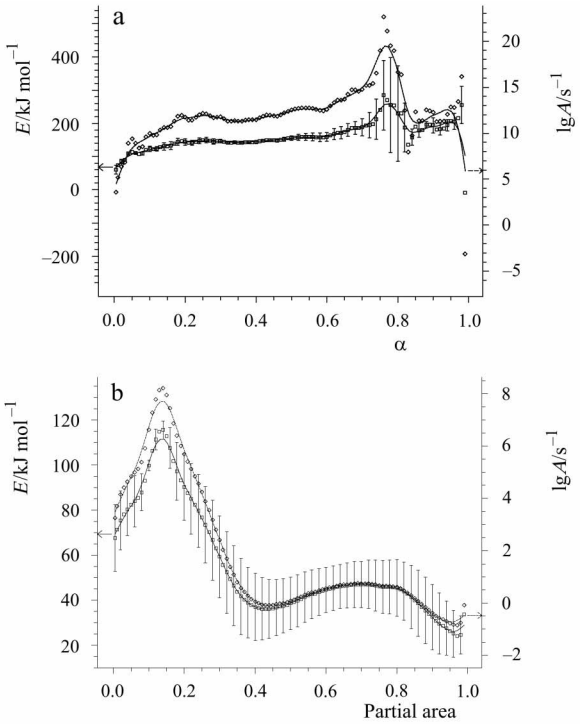

Fig. 5 Arrhenius parameters derived from the Friedman analysis for the oxidation of magnetite; A – TG; B – DSC

Table 4 Selected results from the Flynn–Ozawa model-free kinetic analyses

Technique	E_a/kJ mol^{-1}	log$A$/s^{-1}
TG	225–55	17.4–2.2
DSC	96–38	6.4–0

Clearly there is no hope of fitting a single reaction to what is obviously a multiple step reaction as indicated in Figs 1–3. Hence, the results from a simple linear regression are not included. However, non-linear regression models offer a wide variety of choices. Reasonable discretion must be exercised as discussed in an earlier publication [1]. Because it has been established previously that γ-Fe_3O_4 is an intermediate in this oxidation process, attempts were made to fit a range of two- and three-step processes to the data based on the presence of an intermediate and information derived from the model-free results.

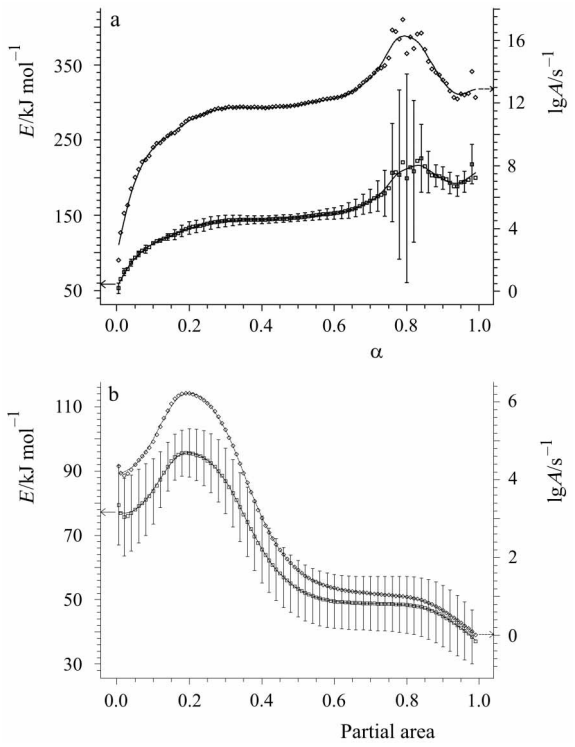

Fig. 6 Arrhenius parameters derived from the Flynn–Ozawa analysis for the oxidation of magnetite; A – TG; B – DSC

Table 5 Selected kinetic results derived from non-linear regression using the two-step consecutive mechanism based on Eq. (1)

Technique	R^2	E_{a1}/ kJ mol^{-1}	logA_1/ s^{-1}	E_{a2}/ kJ mol^{-1}	logA_2/ s^{-1}
TG	0.9989	135	9.75	167	9.29
DSC	0.9525	143	11.4	49.2	4.97

Table 6 Selected kinetic results derived from non-linear regression using the branching mechanism based on Eqs (1) and (2) having *n*-order based reactions

Technique	R^2	E_{a1}/ kJ mol^{-1}	logA_1/ s^{-1}	E_{a2}/ kJ mol^{-1}	logA_2/ s^{-1}	E_{a3}/ kJ mol^{-1}	logA_3/ s^{-1}
TG	0.9997	142	11.7	95.5	8.18	174	11.9
DSC	0.9780	115	8.22	160	12.6	56.0	1.67

Table 7 Selected kinetic results derived from non-linear regression using the branching mechanism based on Eqs (1) and (2) having *n*-order based reactions

Technique	n_1	n_2	n_3
TG	1.79	9.86	2.41
DSC	2.57	1.14	1.49

Table 8 Selected kinetic results derived from non-linear regression using the branching mechanism based on Eqs (1) and (2) having 3D diffusion based reactions

Technique	R^2	E_{a1}/ kJ mol^{-1}	logA_1/ s^{-1}	E_{a2}/ kJ mol^{-1}	logA_2/ s^{-1}	E_{a3}/ kJ mol^{-1}	logA_3/ s^{-1}
TG	0.9992	191	14.6	116	7.77	140	7.23
DSC	0.9440	152	11.0	156	11.6	56.0	0.636

Table 9 Selected kinetic results derived from non-linear regression using the mechanism based on Eq. (3) having 3D diffusion based reactions

Technique	R^2	E_{a1}/ kJ mol^{-1}	logA_1/ s^{-1}	E_{a2}/ kJ mol^{-1}	logA_2/ s^{-1}	E_{a3}/ kJ mol^{-1}	logA_3/ s^{-1}
TG	0.9994	119	8.92	173	13.3	168	9.36
DSC	0.9620	136	10.3	133	9.75	74.4	1.96

Results from the non-linear analysis of simple consecutive reactions, Eq. (1), are summarized in Table 5. Results selecting two branching mechanisms based on simultaneous reactions 1 and 2 are summarized in Tables 6, 7 and 8. The two choices are derived from the best fitting model having all *n*-order reactions and a mode consistent with the best fitting two-step model having all 3D diffusion based mechanisms. Finally another three-step process was selected derived from three consecutive reac-

tions, as indicated by Eq. (3) using all 3D diffusion based reactions. Clearly γ-Fe_2O_3 is either X or Y. The consumption of O_2 in this scheme may take place over more than one step. The results are summarized in Table 9.

$$2Fe_3O_4+O_2 \rightarrow 3\gamma\text{-}Fe_2O_3 \rightarrow 3\alpha\text{-}Fe_2O_3 \quad (1)$$

$$2Fe_3O_4+O_2 \rightarrow 3\alpha\text{-}Fe_2O_3 \quad (2)$$

$$2Fe_3O_4+O_2 \rightarrow X \rightarrow Y \rightarrow 3\alpha\text{-}Fe_2O_3 \quad (3)$$

Discussion

Temperatures at the peak positions for the two steps summarized in Table 1 show a fair correspondence between the DTG and DSC peaks, particularly for the first peak. The average total mass gain is 3.47%, in excellent agreement with the theoretical mass gain of 3.46% for Eq. (1). The point of inflection between the two steps is consistent at a value of α=0.80±0.02. No obvious intermediate or reason for a change in mechanism is associated with that particular stoichiometry. The second DSC peak clearly has a significant mass gain associated with it, so that it can not be attributed to simply the γ to α transition as has been claimed [4].

Applying model-free kinetics to the full range of the oxidation, as was done here, would seem to be doomed to failure in view of the clear steps in both the TG and DSC results presented in Figs 1–3 and Table 1. The ASTM approach is somewhat different, however, in that it focuses on a single point in the reaction, i.e., the maximum rate. Consequently, it is looking at a very narrow range of α (around 0.4, in this case) corresponding to the first major step of the reaction. Those results in Table 2 should therefore be more meaningful and comparable to the more flexible non-linear fits associated with that particular step of the reaction. The results for the TG and DSC are also in good agreement with each other for the ASTM approach in contrast to the other model-free methods.

The Friedman and Flynn–Ozawa approaches, on the other hand, attempt to look at the whole range of α and thus would be expected to show wide divergence, Figs 5 and 6 plus Tables 3 and 4. The parameters for the analyses of the TG and DSC data are very different. In addition, the relationships between these values during the first and second peaks in the reaction are inconsistent. The TG results indicate higher values for the second reaction, while the DSC conclusions are the opposite.

For this complex overall reaction it is therefore more reasonable to concentrate on the non-linear regression analyses. General inspection of both the TG and DSC curves in Figs 1–3 clearly suggests a well-resolved two-step process for the oxidation. Very close inspection, however, further suggests the possibility of yet a small third step in the early stage of the reaction. The effect of γ-Fe_2O_3 as an intermediate in these processes is difficult to assess from the TG curves because the mass change associated with its formation and that of the final product are identical. Neither do the DSC curves indicate any sharp exotherm superimposed on an overall two- or three-step exothermic oxidation process. Thus the simplistic steps invoked in Eqs 1 and 2

can not be used to explain these multi-step mechanisms. There are either partially oxidized amorphous type intermediates or other physical reasons for the changes in mechanism during the course of the reaction.

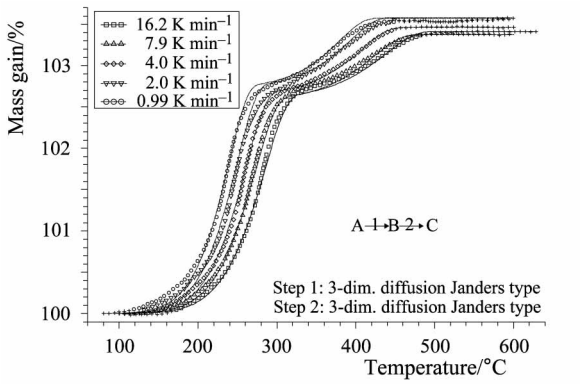

Fig. 7 Fit for the non-linear regression of the TG kinetic data for the two-step oxidation of magnetite. Both steps invoke the 3D diffusion Jander equation

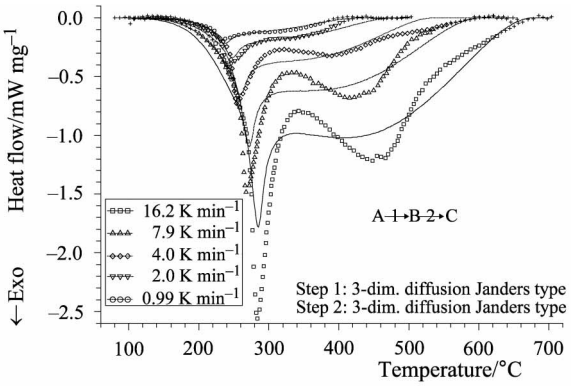

Fig. 8 Fit for the non-linear regression of the DSC kinetic data for the two-step oxidation of magnetite. Both steps invoke the 3D diffusion Jander equation

The best fitting two-step mechanism involved 3D diffusion, the Jander equation for each step. The degree of fit based on the results in Table 5 is indicated in Fig. 7 for the TG data. Except for the small departures at the very beginning and those in the transition region, the fit is generally good. Figure 8 shows the analogous fit to the DSC data. Obviously, as indicated by the low value of R^2, it is a very poor fit everywhere, particularly in the area of the second stage. This mechanism might be explained by an approach similar to that defined by Eq. 1, where the first reaction is incomplete. If after about 70–80% of the reaction (α= 0.7–0.8) the γ form of the product converts to the α form, the remainder of the reaction then proceeds without formation of an intermediate.

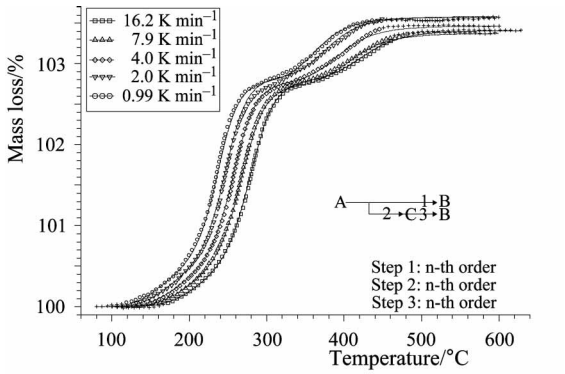

Fig. 9 Fit for the non-linear regression of the TG kinetic data for the three-step branching oxidation of magnetite. All steps invoke the *n*-order equation

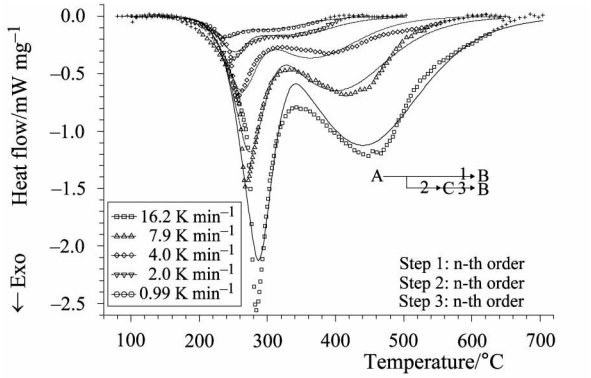

Fig. 10 Fit for the non-linear regression of the DSC kinetic data for the three-step branching oxidation of magnetite. All steps invoke the *n*-order equation

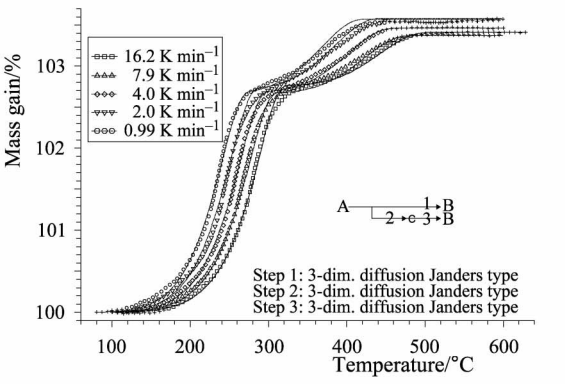

Fig. 11 Fit for the non-linear regression of the TG kinetic data for the three-step branching oxidation of magnetite. All steps invoke the 3D diffusion Jander equation

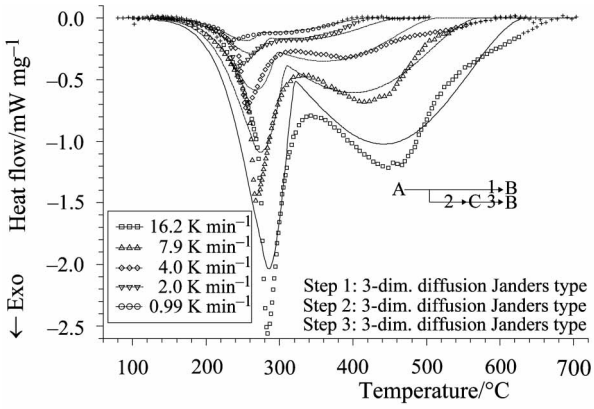

Fig. 12 Fit for the non-linear regression of the DSC kinetic data for the three-step branching oxidation of magnetite. All steps invoke the 3D diffusion Jander equation

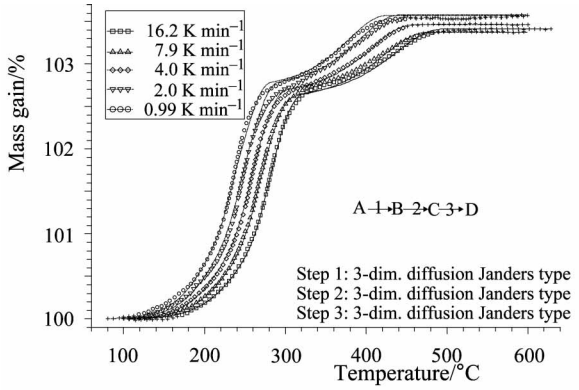

Fig. 13 Fit for the non-linear regression of the TG kinetic data for the three-step consecutive oxidation of magnetite. All steps invoke the 3D diffusion Jander equation

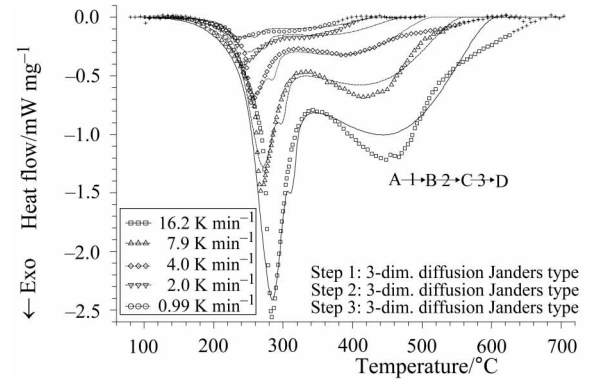

Fig. 14 Fit for the non-linear regression of the TG kinetic data for the three-step consecutive oxidation of magnetite. All steps invoke the 3D diffusion Jander equation

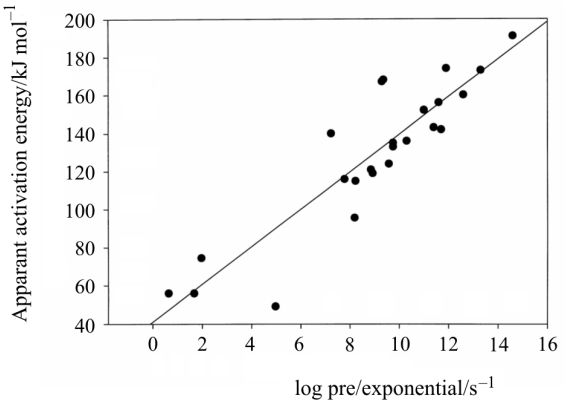

Fig. 15 Kinetic compensation plot for the oxidation of magnetite

As was stressed earlier [1], moving to three-step processes, either branching or consecutive, adds additional freedom that must improve the resulting fit. The question remains as to its justification. The best fitting three-step mechanism employed a branching set of *n*-order equations for each step and is represented by the parameters in Tables 6 and 7. The high degree of fit is indicated in Fig. 9 for the TG data. Although the fit to the DSC data is much better, Fig. 10, it still does not approach that observed for the TG data. One is tempted to explain the branching aspect by the simultaneous oxidation to both the α and γ forms, however, there is not an obvious explanation for the third step. There also does not appear to be any significance to attach to the observed orders of the reaction in Table 7.

The markedly improved fit of the three-step mechanism for DSC analyses compared to that for TG is in complete accord with the contention that the DSC data require an additional reaction to account for the γ to α conversion which involves the evolution of heat but no mass gain.

In order to make a more direct comparison of the two- and three-step processes, fits were made based on the same 3D Jander equations used in the two-step analysis to both three-step branching and consecutive reactions. The resulting fits using the parameters given in Tables 8 and 9 are shown in Figs 11–14. The TG data fit nearly as well in both instances, however, the fits to the DSC data are clearly inferior.

Conclusions

It is very difficult to derive any major insights into the oxidation processes from this study of the heterogeneous kinetics beyond the obvious fact of its complexity. Work on $CaCO_3$ [1] and the excellent studies by Anderson *et al.* [6, 7] on $CaC_2O_4{\cdot}2H_2O$ also elaborate on these issues of comparing TG and DSC results along with the questions concerning optimal curve fitting. In this instance again the results based on the TG data appear much more reliable than those based on the simultaneous DSC data. The considerable improvement achieved by a third step in the analysis of the DSC data does suggest the effect of the metastable to stable conversion on the DSC data.

Figure 15 is a plot of the kinetic parameters from Tables 2 and 5–9 in the form of a kinetic compensation plot. The very existence of this virtually omnipresent correlation implies uncertainty in arriving at a unique set of Arrhenius parameters, much less assigning any particular significance to the values selected [8]. There is also no reason for the activation energy and pre-exponential terms to track each other as a function of α such as seen in Figs 5 and 6, since they are presumably totally independent variables. One is tempted to report the mean values associated with such a compensation plot, approximately 120 kJ mol^{-1} and 8 s^{-1}. This, however, does not reflect the obvious multi-step nature of the process. Consequently, the authors prefer the simple two-step analysis to explain the oxidation process, but offer no explanation for the change in mechanism. The slight improvement in fit achieved using three-step processes does not seem warranted and provides no additional insights.

Note added in proof

The formation of the γ-Fe_2O_3 intermediate in the appropriate temperature regime has been recently confirmed by thermomagnetometry. It appears as a note in Thermochimica Acta 73 (2003) in press by J. P. Sanders and P. K. Gallagher.

References

1 J. P. Sanders and P. K. Gallagher, Thermochim. Acta, 388 (2002) 115.
2 P. K. Gallagher, E. M. György and H. E. Bair, J. Chem. Phys., 71 (1979), 830.
3 The Making, Shaping and Treating of Steel 9th Edition, Ed., Harold E. McGannon, United States Steel Corporation, Pittsburgh, PA 1970.
4 W. Frömming, in 'Thermal Analysis Vol. 1', I. Buzás, Ed., Heyden Son., London 1974, p. 751.
5 J. Opffermann, J. Therm. Anal. Cal., 60 (2000) 641.
6 H. L. Anderson, A. Kemmler, G. W. H. Höhne, K. Heldt and R. Strey, Thermochim. Acta, 332 (1999) 33.
7 H. L. Anderson, R. Strey, G. W. H. Höhne, A. Kemmler and K. Heldt, Thermochim. Acta, 332 (1999) 33.
8 M. E. Brown and A. K. Galwey, Thermochim. Acta, 387 (2002) 173.